Nanoscale

www.rsc.org/nanoscale

Volume 5 | Number 14 | 21 July 2013 | Pages 6189–6608

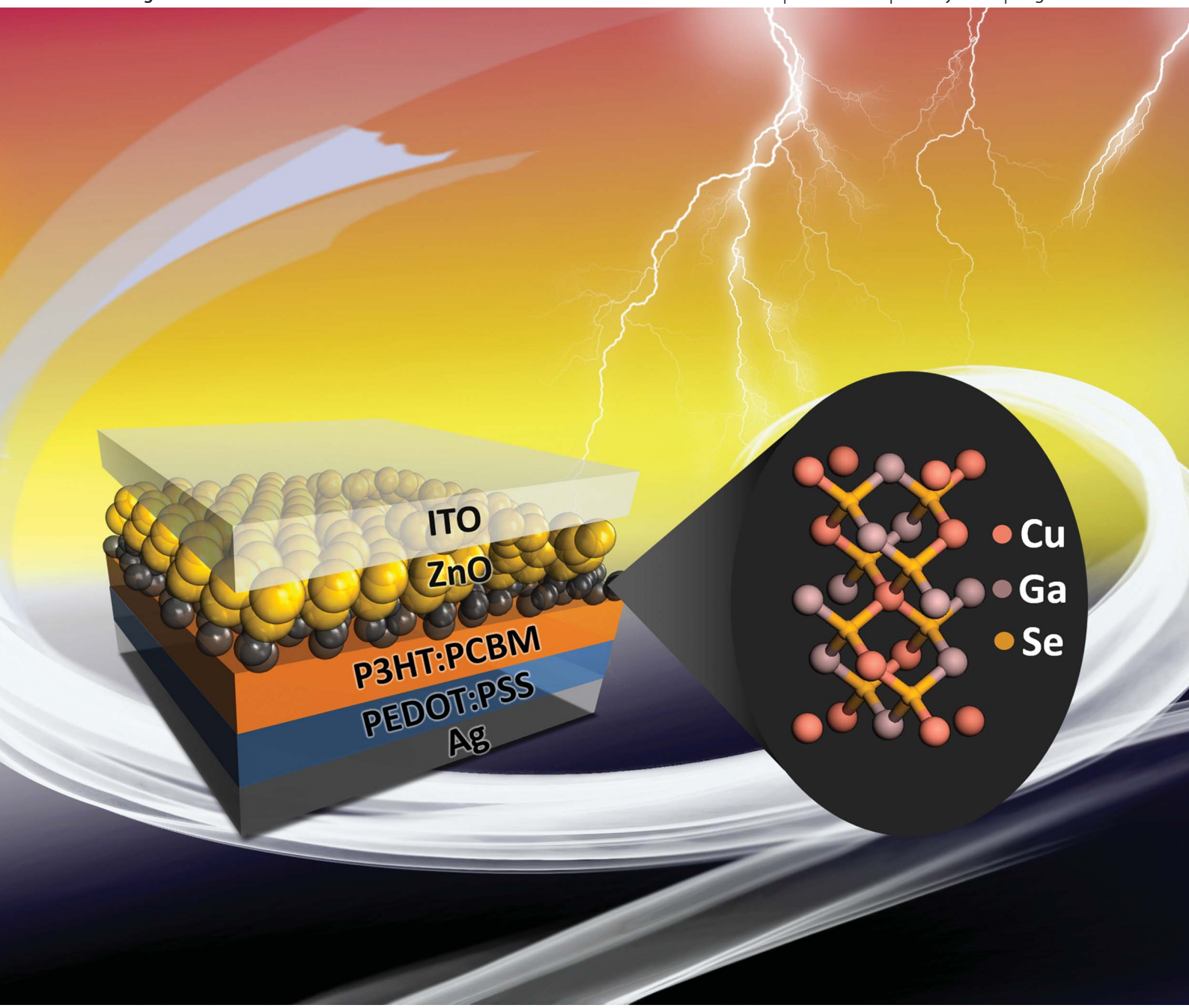

ISSN 2040-3364

RSC Publishing

PAPER

He *et al.*

An energy-harvesting scheme employing $CuGaSe_2$ quantum dot-modified ZnO buffer layers for drastic conversion efficiency enhancement in inorganic–organic hybrid solar cells

NCNST

Nanoscale

RSC Publishing

PAPER

An energy-harvesting scheme employing $CuGaSe_2$ quantum dot-modified ZnO buffer layers for drastic conversion efficiency enhancement in inorganic–organic hybrid solar cells†

Cite this: *Nanoscale*, 2013, **5**, 6350

Cherng-Rong Ho,[a] Meng-Lin Tsai,[a] Hung-Jun Jhuo,[b] Der-Hsien Lien,[a] Chin-An Lin,[a] Shin-Hung Tsai,[a] Tzu-Chiao Wei,[a] Kun-Ping Huang,[c] Show-An Chen[b] and Jr-Hau He*[a]

Received 17th December 2012
Accepted 30th January 2013

DOI: 10.1039/c3nr34155k

www.rsc.org/nanoscale

We demonstrated a promising route to enhance the performance of inverted organic photovoltaic (OPV) devices by the incorporation of $CuGaSe_2$ (CGS) quantum dots (QDs) into the ZnO buffer layer of P3HT:PCBM-based devices. The modification of QDs provides better band alignment between the organic/cathode interface, improves ZnO crystal quality, and increases photon absorption, leading to more effective carrier transport/collection. By employing this energy-harvesting scheme, short-circuit current density, open-circuit voltage, and fill factor of the OPV device after CGS QD modification are improved by 9.43%, 7.02% and 6.31%, respectively, giving rise to a 23.8% enhancement in the power conversion efficiency.

Introduction

Organic photovoltaics (OPVs) have attracted great attention to become a promising candidate for future energy sources due to their low-cost, high-performance, and mechanically flexible properties and reached 6–8% for the conventional devices (substrate/hole selective contact/active layer/electron selective contact).[1–3] Typically, the conventional device structure is sandwiched by poly(3,4-ethylenedioxylenethiophene):polystyrene sulfonic acid (PEDOT:PSS) on indium tin oxide (ITO) glasses as the anode and the low-work-function metal, such as Al, as the cathode. However, PEDOT:PSS on ITO glasses is unstable since indium contaminates the polymer and thus degrades the OPV performance rapidly.[4] Accordingly, an inverted device structure has been adopted to alleviate this stability problem.[5–8] Moreover, the ideal process for inverted solar cell fabrication would be to use solution-processing techniques to deposit the different layers in the solar cell and is thus more compatible with roll-to-roll manufacturing processes than that for the conventional cell. In the inverted structure, the carrier-collection nature of the electrodes is reversed, with a high-work-function metal (such as Au and Ag) as the anode and the ITO electrode as the cathode. As compared to the conventional ones, inverted device architectures tend to exhibit low fill factor (FF) and photocurrent, leading to unsatisfactory conversion efficiency.[5–10]

For resolving the issue of low FF and photocurrent in an inverted structure, much effort has been focused on the optimization of morphologies and electronic structures of active materials by developing advanced processing methods for superior optical absorption and charge separation,[2,11–13] improving the interface between contact electrodes and active materials,[13–16] and understanding underlying device physics.[2,11–16] One of the major focuses is to use some of the buffer (or interfacial) layers to modify the ITO interface to decrease the work function for efficiently collecting electrons since the work function of ITO is usually not aligned with the lowest unoccupied molecular orbital (LUMO) of fullerenes. The most popular n-type buffer layers are TiO_2 and ZnO that enable the unipolar extraction of photogenerated electrons from the active layers to the ITO electrodes.[17–22] Even though reasonable efficiencies have been reached with TiO_2 and ZnO buffer layers in inverted solar cells, the development of interfacial engineering in inverted solar cells is being intensely pursued. For example, Lin *et al.* have reported that the ZnO/P3HT interface after molecular modification can play the role of assisting charge separation and preventing back recombination.[23] Self-assembled-monolayer-modified ZnO/metals as cathodes show dramatic improvements in efficiencies.[24] These approaches could be beneficial for the future development of printable solar cells. Furthermore, 3D structures of metal oxide have been demonstrated to be another approach to improve the power conversion efficiency (PCE) since the increased interface of the acceptor/buffer layer improves the electron transport and is expected to allow for thicker active layers.[25–29]

[a]*Institute of Photonics and Optoelectronics, and Department of Electrical Engineering, National Taiwan University, Taipei, Taiwan. E-mail: jhhe@ntu.edu.tw; Fax: +886-2-2367-7467; Tel: +886-2-3366-9646*

[b]*Department of Chemical Engineering, National Tsing Hua University, Hsinchu, Taiwan*

[c]*Mechanical and Systems Research Labratories, Industrial Technology Research Institute, Hsinchu, Taiwan*

† Electronic supplementary information (ESI) available: The X-ray diffraction and PL spectrum of $CuGaSe_2$ quantum dots. See DOI: 10.1039/c3nr34155k

This journal is © The Royal Society of Chemistry 2013

In this work, sol–gel ZnO films modified with $CuGaSe_2$ (CGS) quantum dots (QDs) using a spin coating method could serve as effective buffer layers for poly(3-hexylthiophene) (P3HT):(6,6)-phenyl-C61-butyric acid methyl ester (PCBM) OPVs. CGS QDs on the ZnO buffer layers are able to suppress carrier recombination and increase electron collection efficiency *via* (i) a better energy level alignment at the organic/cathode interface by lowering the metal work function, (ii) improving the crystal quality of ZnO, and (iii) increasing the photon absorption. By modifying sol–gel ZnO buffer layers with CGS QDs with the concentration of 6×10^{-3} wt%, P3HT/PCBM OPV cells exhibit improved short-circuit current density (J_{SC}) from 10.73 to 11.74 mA cm^{-2}, open-circuit voltage (V_{OC}) from 0.57 to 0.61 V, and fill factor (FF) from 53.53 to 56.91%, giving rise to the PCE enhancement of 23.8%. This solution process-implemented technique provides an efficient method for interface engineering in organic-based flexible optoelectronic devices.

Experimental

We first prepared a solution of Zn precursor by dissolving zinc acetate ($Zn(CH_3CO_2)_2 \cdot 2H_2O$) in 2-methoxyethanol ($C_3H_8O_2$, 2MOE) and monoethanolamine (C_2H_7NO, MEA). The solution was stirred at 60 °C for 2 hours to yield a homogeneous solution. The synthesis of CGS QDs was conducted in a solvothermal process with a stoichiometric mixture of selenium, copper, and $Ga(NO_3)_3$ (99.8%). All precursors with a solvent of ethylenediamine were loaded into a 50 mL Teflon-lined autoclave. The autoclave was sealed and heated to 200 °C for 48 hours. After cooling down to room temperature, the precipitate was filtered, washed with DI water and ethanol, and then dried under vacuum at 120 °C for 4 hours. The CGS QDs were dispersed in isopropyl alcohol (IPA) with various concentrations.

After cleaning the ITO-coated glass substrate, the sol–gel ZnO was spun four times with a spin-coater at 3000 rpm for 10 seconds each time to yield a 100 nm-thick film. The deposited films were thermally treated at 150 °C for 3 minutes in each deposition. CGS QDs in IPA with 2×10^{-3} to 3×10^{-1} wt% were spin-coated on the ZnO layer at a speed of 3000 rpm for one time. The sample was then annealed in air for 1 hour at 450 °C. Then a polymer blend of P3HT:PCBM (Batron AI 4083) (weight ratio of 1 : 1) was spin-coated on top of the CGS layer from a 20 mg mL^{-1} *o*-dichlorobenzene (ODCB) solution at 600 rpm in glove box and dried in covered glass Petri dish (solvent annealing). Then PEDOT:PSS solution was prepared as a hole transporting layer and deposited by spin-coating method at 5000 rpm for 30 seconds. After annealing these samples for 10 minutes at the temperature of 140 °C, 100 nm thick Ag layers were deposited by thermal evaporation through a shadow mask to define a device area of 0.1 cm^2.

Results and discussion

Fig. 1(a) shows the schematic of the device structure layout and the chalcopyrite crystal structure of CGS QDs. CGS QDs were dispersed at ZnO buffer layers before depositing P3HT:PCBM. The energy level diagram of the device is depicted in Fig. 1(b). The conduction band minimum (CBM) of CGS QDs lies between the LUMO of PCBM and the CBM of ZnO, creating a cascade band structure from PCBM to ZnO. The decrease in band offset at the interface between electrodes and active layers could facilitate effective carrier transfer, reducing the rate of surface recombination and thus enhancing the carrier collection efficiency.[30,31] Fig. 1(c) shows the absorbance spectrum of pure CGS QDs measured by a UV-VIS-NIR spectrophotometer (JASCO V-670). Due to the bandgap of 1.78 eV for CGS QDs, the absorbance is gradually increased at the wavelengths shorter than 700 nm.

The X-ray diffraction spectrum of the as-synthesized CGS QDs is shown in Fig. S1 in the ESI† for characterizing the microstructure of CGS QDs. The diffraction peaks were identified to be chalcopyrite crystal structure based on the standard file (JCPDS 81-0903). The average QD diameter was calculated to be ~7.1 nm based on Scherrer's formula:[32]

$$D = \frac{0.93\lambda}{\beta \cos\theta} \quad (1)$$

where D is the average QD diameter (nm), λ is the incident X-ray wavelength (nm), β is the full width at half maximum in

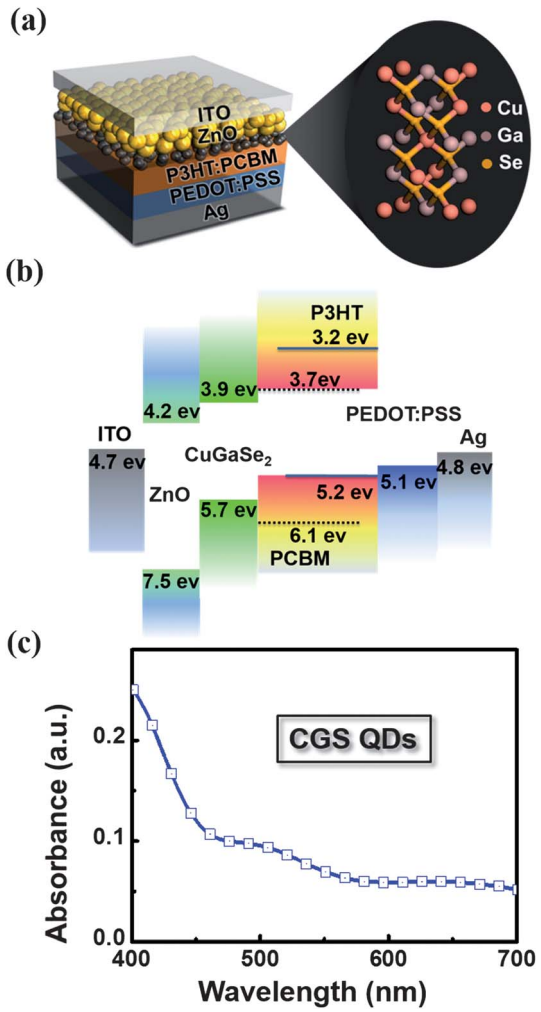

Fig. 1 (a) Device structure and (b) energy level diagram of the components of the CGS QD-modified P3HT:PCBM OPV. (c) UV-visible absorption spectra of CGS QDs.

radians, and θ is the Bragg angle. From the photoluminescence (PL) spectrum shown in Fig. S2,† the bandgap of CGS QDs is ~1.78 eV, which is larger than that of bulk CGS (1.68 eV). The increased bandgap could be attributed to the elimination of surface states and the quantum confinement effect.[33] The scanning electron microscopy (SEM) images of ZnO films without and with CGS QDs annealed at 450 °C for 1 h in air are shown in Fig. 2(a) and (b), respectively. It is clearly shown that ZnO films with CGS QDs exhibit larger grain size; the average grain size for CGS QD-coated ZnO films is 52 nm, which is larger than that of 28 nm for pure ZnO films, implying that the CGS QDs play a role in the grain growth during the annealing process. Fig. 3(a) shows the XRD spectra of ZnO films with and without CGS QDs. Strong peaks located around 34.45° correspond to the diffraction from (0002) plane of ZnO. According to the full-width-at-half-maximum change in the peak at 34.45°, it is shown that grain size is increased after CGS QD modification, echoing the SEM observation in Fig. 2. It is expected that ZnO films with larger grain sizes would provide better wettability and enhance adhesion with the active layer.[34] By employing ZnO films with larger grain sizes, grain boundaries on electron transfer pathways should also be reduced to prevent photoexcited carriers from being captured by the large amount of defects present in grain boundaries. The underlying mechanism for improved ZnO crystal quality after employing CGS QDs could be explained as follows. Due to the non-stoichiometric nature of ZnO, it has been reported that doping with Al, Ga or incorporation of nanoparticles into ZnO can increase grain size.[35] It has been also been reported that chalcopyrite materials could be used as catalysts to induce the decomposition of solvents such as alcohols decomposed into highly volatile ketone or alkane due to dehydrogenation or dehydration reactions.[36,37] During annealing, CGS QDs, one of chalcopyrite materials, accelerate the decomposition of organic solvents and residuals, resulting in higher ZnO crystallization rate and thus better ZnO crystal quality.

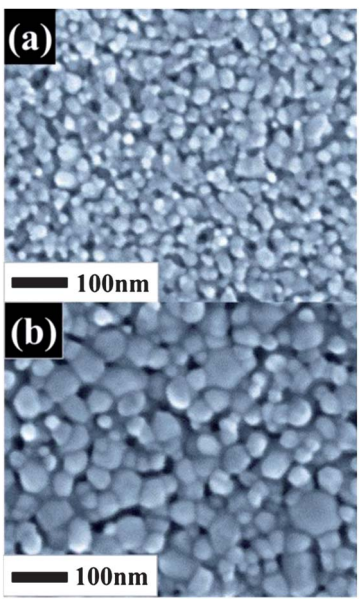

Fig. 2 SEM images of (a) pure sol–gel ZnO buffer layers and (b) sol–gel ZnO buffer layers modified with CGS QDs.

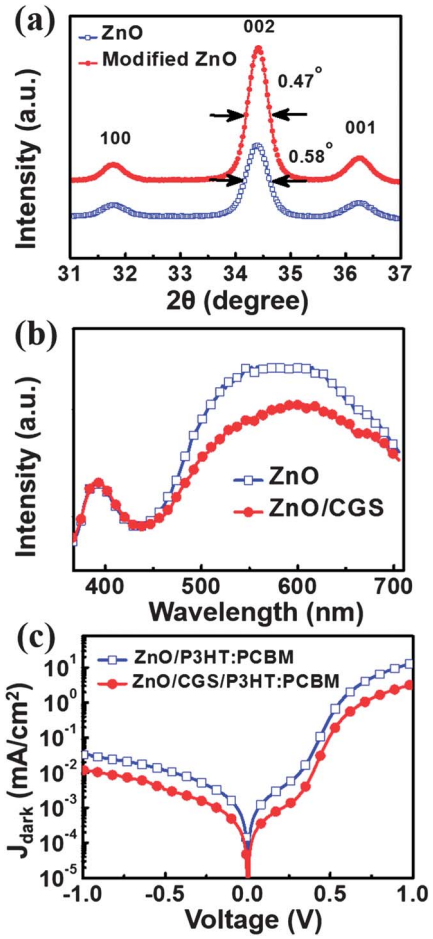

Fig. 3 (a) XRD and (b) PL spectra for sol–gel ZnO buffer layers before and after CGS QD modification. (c) Dark current densities of OPV devices with and without CGS QD modification.

Fig. 3(b) depicts PL spectra of ZnO buffer layers before and after CGS QD modification. Near-bandedge emission (NBE) and deep-level emission (DLE) of ZnO are located at 390 nm and 600 nm. It is worth noting that the DLE peak, which corresponds to the emission due to native defects originating from ZnO,[38,39] is reduced after CGS QD modification. This is because CGS QDs could effectively eliminate the surface states of ZnO by decreasing the density of grain boundary. Therefore, the event of the photoexcited carrier trapping at ZnO surfaces is expected to be decreased under solar light illumination, which will be confirmed later. Decreased density of grain boundary also results in the suppression of dark current due to the elimination of conducting paths, as shown in Fig. 3(c). In a solar device, the magnitude of V_{OC} is closely related to that of J_{dark}. The devices with a low recombination rate usually exhibit a low dark current density, giving rise to a high value of V_{OC}, which will be discussed later as well.

The external quantum efficiency (EQE) spectrum of OPV devices measured by a solar cell spectral response measurement system (Enli SR-156), as shown in Fig. 4(a), shows an efficiency improvement after CGS QD modification of a concentration of

This journal is © The Royal Society of Chemistry 2013

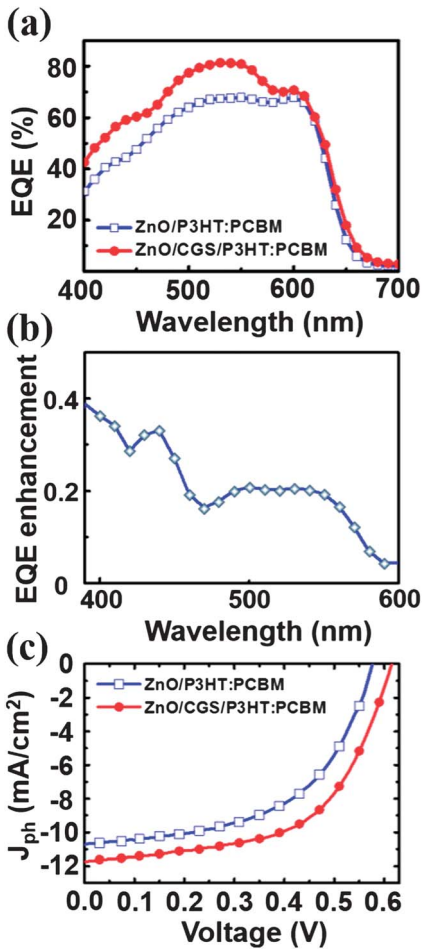

Fig. 4 (a) EQE spectra of OPVs with and without CGS QD modification. (b) EQE enhancement of OPVs with CGS QD modification, and (c) *J–V* characteristics of the photovoltaic devices with and without CGS QDs under AM 1.5G illumination.

6×10^{-3}% at the interface between P3HT:PCBM and ZnO. As shown in Fig. 4(b), we define the EQE enhancement as $(EQE_{with\ QDs} - EQE_{w/o\ QDs})/EQE_{w/o\ QDs}$ obtained from Fig. 4(a). The uniform broadband increase in EQE will be expected if CGS QDs only promote the efficiency of electron transport/collection *via* improving crystal quality of ZnO buffer layers and providing the cascading energy band structure, where the CBM of CGS QDs is higher than CBM of ZnO and lower than the LUMO of PCBM. However, one can see that the EQE enhancement increases with decreased wavelengths and is closely related to the CGS QDs absorption spectrum shown in Fig. 1(c), indicating that the EQE enhancement is partly attributed to the absorptivity of CGS QDs. This is also supported by increased absorption with decreased wavelength appearing in the corresponding absorbance spectra of the OPV devices shown in Fig. S3(a).† The pronounced absorption enhancement of devices with QDs at wavelengths shorter than 500 nm also confirms the effect of increased absorptivity at shorter wavelengths. The spectrum of absorbance (*A*) enhancement, which is defined as $(A_{with\ QDs} - A_{w/o\ QDs})/A_{w/o\ QDs}$, is shown in Fig. S3(b).† The spectrum is also closely related to Fig. 1(c) and further supports the idea of the increased EQE enhancement at shorter wavelengths being partially attributed to the enhanced absorption of QDs in the shorter wavelength region.

In order to emphasize the relation between device performance and QD concentration, the performances of OPV devices with various QD concentrations (from 2×10^{-3} to 3×10^{-1}%) are summarized in Table 1. The devices were characterized with one-sun AM 1.5G light with a power density of 100 mW cm^{-2} and a digital source meter (2400, Keithley). The device with CGS QD concentration of 6×10^{-3}% shows the highest PCE, which can be seen in the current density–voltage (*J–V*) characteristics of the cells under illumination, shown in Fig. 4(c). The results indicate that CGS QDs of 6×10^{-3}% improved the PV performance of the devices, especially on FF and J_{SC}. In contrast to monotonic increase of J_{SC} with the QD concentration due to a cascade band structure from PCBM to ZnO and enhanced absorption, FF reaches a maximum value at a concentration of 6×10^{-3}%. It is known that FF is affected by series resistance (R_s) and shunt resistance (R_{sh}).[40] The increased FF of cells with CGS QDs lower than 6×10^{-3}% is attributed to the increased R_{sh} since the appropriate amount of CGS QDs eliminates the leakage paths *via* the grain growth of ZnO and prevents holes excited in the P3HT from reaching the ZnO surface to recombine with electrons in the ZnO. As the QD concentration is further increased, CGS QDs would aggregate within the ZnO surface and thus result in the inferior morphology of active layers, leading to a decrease of R_{sh}.[41] Moreover, the conductivity of CGS QDs is much lower than that of ZnO.[42] Therefore, the R_s of the device increases with the concentration of CGS QDs, leading to a substantial decrease in FF. Based on the evolution of R_s and R_{sh}, the maximum of FF at a QD concentration of 6×10^{-3}% is obtained. Theoretically, the value of V_{OC} for a polymer solar cell is expressed by the empirical equation

$$V_{OC} = e^{-1} \times \left(\left| E_{HOMO}^{donor} \right| - \left| E_{LUMO}^{acceptor} \right| - 0.3\ eV \right) \quad (2)$$

where *e* is the elementary charge, E_{HOMO}^{donor} is the highest occupied molecular orbital (HOMO) level of the donor, $E_{LUMO}^{acceptor}$ is the LUMO level of the acceptor, and 0.3 eV is an empirical value for efficient charge separation.[7,43,44] This implies that the value of V_{OC} is only influenced by the band offset between the electron donor and acceptor species and thus leads to the fact that many scientists have focused on developing new polymer composite layers for high V_{OC} of OPV cells, which could be costly, time-consuming, and complicated. However, V_{OC} is also affected by

Table 1 Photovoltaic parameters of the OPV incorporated with CGS QDs under one-sun AM 1.5G illumination

Concentration of CGS QDs (wt%)	J_{sc} (mA cm^2)	V_{oc} (V)	FF (%)	R_{sh} (kΩ cm^2)	R_s (Ω cm^2)	PCE (%)
0	10.73	0.57	53.53	0.2398	9.5238	3.32
2×10^{-3}	11.19	0.57	52.51	0.3137	10.2371	3.35
6×10^{-3}	11.74	0.61	56.91	0.6334	10.3617	4.11
1×10^{-2}	11.80	0.60	54.36	0.4734	10.4727	3.85
4×10^{-2}	11.82	0.60	52.85	0.3927	10.6239	3.76
8×10^{-2}	11.86	0.60	51.86	0.3462	11.0325	3.69
3×10^{-1}	12.02	0.60	50.35	0.3451	12.3779	3.63

non-radiative recombination pathways. Further eliminating these non-radiative pathways *via* improving the crystal quality of ZnO by introducing CGS QDs with the concentration higher than 6×10^{-3}% improves V_{OC}.[7,44] Briefly, by employing CGS QD modification with the concentration of 6×10^{-3}%, the device with ZnO buffer layers achieves the increase of J_{SC} from 10.73 to 11.74 mA cm^2, FF from 53.53 to 56.91% and V_{OC} from 0.57 to 0.61 V, which is significant PCE enhancement of 23.8%. We do note that all of the OPV process conditions and photovoltaic parameters are correlated with each other, and therefore an accurate optimization of interface and each layer composing the OPV device will strictly be demanded in order to avoid efficiency loss and to achieve the best performance.

Conclusion

In conclusion, a feasible energy-harvesting scheme employing CGS QDs on ZnO buffer layers in inverted OPV cells was demonstrated *via* (i) efficient electron transfer from P3HT:PCBM bulk heterojunction toward ITO layers due to a cascade band structure from PCBM, ZnO to ITO, (ii) improving crystal quality of ZnO buffer layers, and (iii) enhancing absorption efficiency due to the high absorption coefficient of CGS QDs. Altering the concentration of CGS QDs allows understanding of underlying device physics. An optimal condition at the concentration of 6×10^{-3}% achieves the increase of J_{SC} from 10.73 to 11.74 mA cm^2, FF from 53.53 to 56.91% and V_{OC} from 0.57 to 0.61 V, giving rise to an enhancement of PCE of 23.80%. The solution-based technique for an energy-harvesting scheme demonstrated here shows potential large-scale production of these inverted-based OPV cells.

Acknowledgements

This work was supported by National Science Council of Taiwan (99-2622-E-002-019-CC3, 99-2112-M-002-024-MY3, 101-2622-E-002-012-CC3, and 99-2120-M-007-011) and National Taiwan University (10R70823).

Notes and references

1 V. Shrotriya, Y. Yao, G. Li and Y. Yang, *Appl. Phys. Lett.*, 2006, **89**, 063505.
2 J. Y. Kim, K. Lee, N. E. Coates, D. Moses, T. Q. Nguyen, M. Dante and A. J. Heeger, *Science*, 2007, **317**, 222.
3 S. H. Tsai, H. C. Chang, H. H. Wang, S. Y. Chen, C. A. Lin, S. A. Chen, Y. L. Chueh and J. H. He, *ACS Nano*, 2011, **5**, 9501.
4 A. Sharma, S. Watkins, D. A. Lewis and G. Andersson, *Sol. Energy Mater. Sol. Cells*, 2011, **95**, 3251.
5 K. Lee, J. Kim, S. Park, S. Kim, S. Cho and A. Heeger, *Adv. Mater.*, 2007, **19**, 2445.
6 W. J. E. Beek, M. M. Wienk, M. Kemerink, X. N. Yang and R. A. J. Janssen, *J. Phys. Chem. B*, 2005, **109**, 9505.
7 W. J. Ke, G. H. Lin, C. P. Hsu, C. M. Chen, Y. S. Cheng, T. H. Cheng and S. A. Chen, *J. Mater. Chem.*, 2011, **21**, 13483.
8 T. Yang, W. Cai, D. Qin, E. Wang, L. Lan, X. Gong, J. Peng and Y. Cao, *J. Phys. Chem. C*, 2010, **114**, 6849.
9 M. S. White, D. D. Olson, S. E. Shaheen, N. Kopidakis and D. S. Ginley, *Appl. Phys. Lett.*, 2006, **89**, 142517.
10 C. Waldauf, M. Morana, P. Denk, P. Schilinsky, K. Coakley, S. A. Choulis and C. J. Brabec, *Appl. Phys. Lett.*, 2006, **89**, 233517.
11 N. S. Sariciftci, L. Smilowitz, A. J. Heeger and F. Wudl, *Science*, 1992, **258**, 1474.
12 D. Chen, F. Liu, C. Wang, A. Nakahara and T. P. Russell, *Nano Lett.*, 2011, **11**, 2071.
13 S. K. Hau, K. M. O'Malley, Y.-J. Cheng, H.-L. Yip, H. Ma and A. K.-Y. Jen, *IEEE J. Sel. Top. Quantum Electron.*, 2010, **16**, 1665.
14 S. K. Hau, H.-L. Yip, O. Acton, N. S. Baek, H. Ma and A. K.-Y. Jen, *J. Mater. Chem.*, 2008, **18**, 5113.
15 M. S. White, D. C. Olson, S. E. Shaheen, N. Kopidakis and D. S. Ginley, *Appl. Phys. Lett.*, 2006, **89**, 143517.
16 L. Motiei, Y. Yao, J. Choudhury, H. Yan, T. J. Marks, M. E. van der Boom and A. Facchetti, *J. Am. Chem. Soc.*, 2010, **132**, 12528.
17 G. Yu, J. Gao, J. C. Hummelen, F. Wudl and A. J. Heeger, *Science*, 1995, **270**, 1789.
18 R. Steim, S. A. Choulis, P. Schilinsky and C. J. Brabec, *Appl. Phys. Lett.*, 2008, **92**, 093303.
19 A. Hayakawa, O. Yoshikawa, T. Fujieda, K. Uehara and S. Yoshikawa, *Appl. Phys. Lett.*, 2007, **90**, 163517.
20 D. W. Zhao, P. Liu, X. W. Sun, S. T. Tan, L. Ke and A. K. K. Kyaw, *Appl. Phys. Lett.*, 2009, **95**, 153304.
21 F. C. Krebs, S. A. Gevorgyan and J. Alstrup, *J. Mater. Chem.*, 2009, **19**, 5442.
22 G. Li, R. Zhu and Y. Yang, *Nat. Photonics*, 2012, **6**, 153.
23 Y. Y. Lin, Y. Y. Lee, L. Chang, J. J. Wu and C. W. Chen, *Appl. Phys. Lett.*, 2009, **94**, 063308.
24 H.-L. Yip, S. K. Hau, N. S. Baek, H. Ma and A. K.-Y. Jen, *Adv. Mater.*, 2008, **20**, 2376.
25 I. Gonzalles-Valls and M. Lira-Cantu, *Energy Environ. Sci.*, 2009, **2**, 19.
26 W. H. Baek, I. Seo, T. S. Yoon, H. H. Lee, C. M. Yun and Y. S. Kim, *Sol. Energy Mater. Sol. Cells*, 2009, **93**, 1587.
27 Z. Dong, X. Lai, J. E. Halpert, N. Yang, L. Yi, J. Zhai, D. Wang, Z. Tang and L. Jiang, *Adv. Mater.*, 2012, **24**, 1046.
28 J. Du, J. Qi, D. Wang and Z. Tang, *Energy Environ. Sci.*, 2012, **5**, 6914.
29 X. Lai, J. E. Halpert and D. Wang, *Energy Environ. Sci.*, 2012, **5**, 5604.
30 C. A. Lin, K. P. Huang, S. T. Ho, M. W. Huang and J. H. He, *Appl. Phys. Lett.*, 2012, **101**, 213901.
31 L. J. A. Koster, V. D. Mihailetchi and P. W. M. Blom, *Appl. Phys. Lett.*, 2006, **88**, 093511.
32 A. L. Patterson, *Phys. Rev.*, 1939, **56**, 978.
33 A. P. Alivisatos, *Science*, 1996, **271**, 933.
34 A. K. K. Kyaw, X. W. Sun, C. Y. Jiang, G. Q. Lo, D. W. Zhao and D. L. Kwong, *Appl. Phys. Lett.*, 2008, **93**, 221107.
35 C. Hong, H. Park, H. Park and H. J. Chang, *J. Electroceram.*, 2009, **22**, 353.
36 P. Baláž, *React. Kinet. Catal. Lett.*, 1988, **36**, 287.
37 W. T. House and M. Orchin, *J. Am. Chem. Soc.*, 1960, **82**, 639.
38 C. Y. Chen, M. W. Chen, J. J. Ke, C. A. Lin, J. R. D. Retamal and J. H. He, *Pure Appl. Chem.*, 2010, **82**, 2055.

 This journal is © The Royal Society of Chemistry 2013

39 C. Y. Chen, C. A. Lin, M. J. Chen, G. R. Lin and J. H. He, *Nanotechnology*, 2009, **20**, 185605.
40 X. M. Fan, J. S. Lian, Z. X. Guo and H. J. Lu, *Appl. Surf. Sci.*, 2005, **239**, 176.
41 P. Ravirajan, A. M. Peiró, M. K. Nazeeruddin, M. Graetzel, D. D. C. Bradley, J. R. Durrant and J. Nelson, *J. Phys. Chem. B*, 2006, **110**, 7635.
42 M. Law, L. E. Greene, A. Radenovic, T. Kuykendall, J. Liphardt and P. Yang, *J. Phys. Chem. B*, 2006, **110**, 22652.
43 M. C. Scharber, D. Mühlbacher, M. Koppe, P. Denk, C. Waldauf, A. J. Heeger and C. J. Brabec, *Adv. Mater.*, 2006, **18**, 789.
44 K. Vandewal, K. Tvingstedt, A. Gadisa, O. Inganas and J. V. Manca, *Nat. Mater.*, 2009, **8**, 90.

This journal is © The Royal Society of Chemistry 2013